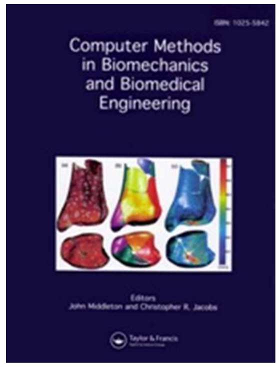

The use of XFEM to assess the influence of intra-cortical porosity on crack propagation

Journal:	*Computer Methods in Biomechanics and Biomedical Engineering*
Manuscript ID	GCMB-2016-0082
Manuscript Type:	Research Article (4,000 words)
Date Submitted by the Author:	29-Feb-2016
Complete List of Authors:	Rodriguez-Florez, Naiara; Imperial College London Carrierio, Alessandra; Florida Institute of Technology Shefelbine, Sandra; Northeastern University,
Keywords:	XFEM, intra-cortical porosity, crack propagation, osteogenesis imperfecta

The use of XFEM to assess the influence of intra-cortical porosity on crack propagation

Naiara Rodriguez-Florez[a], Alessandra Carriero[b], Sandra J. Shefelbine[c*]

[a] *Department of Bioengineering, Imperial College London, London SW7 2AZ, UK. Email: nr211@imperial.ac.uk*

[b] *Department of Biomedical Engineering, Florida Institute of Technology, Melbourne 32901, USA. Email: acarriero@fit.edu*

[c] *Department of Mechanical and Industrial Engineering and Department of Bioengineering, Northeastern University, Boston MA 02115, USA. Email: s.shefelbine@neu.edu*

*Corresponding Author:

Dr Sandra J Shefelbine

Department of Mechanical and Industrial Engineering

Northeastern University

360 Huntington Ave

Boston, MA 02115

s.shefelbine@neu.edu

+1 617-373-3199

Word count: 4000
Figures: 9

Abstract

This study aimed at using eXtended Finite Element Method (XFEM) to characterize crack growth through bone's intra-cortical pores. Two techniques were compared using Abaqus: 1) void material properties were assigned to pores; 2) multiple enrichment regions with independent crack-growth possibilities were employed. Both were applied to 2D models of transverse images of mouse bone with differing porous structures. Results revealed that assigning multiple enrichment regions allows for multiple cracks to be initiated progressively, which cannot be captured when the voids are filled. Therefore, filling pores with one enrichment region in the model will not create realistic fracture patterns in Abaqus-XFEM.

KEYWORDS: XFEM; intra-cortical porosity; microstructure; crack propagation; osteogenesis imperfecta.

1. Introduction

Healthy bone is a tough material because of multiple toughening mechanisms that act from the molecular level up to the whole-bone level (Buehler, 2007; Gupta et al., 2013; Launey et al., 2010; Nalla et al., 2005; Ritchie et al., 2009; Ural and Vashishth, 2014; Wang and Gupta, 2011; Zimmermann et al., 2014). It is still not fully understood how specific diseases and age affect bone's ability to resist fracture at different length-scales. At the tissue level, bone porosity is expected to have a significant influence on bone toughness and crack propagation (Carriero et al., 2014b; Turnbull et al., 2014; Ural and Vashishth, 2014; Voide et al., 2011; Yeni et al., 1997). Pores might promote crack deflection, serve as stress concentration for the creation of new micro-cracks, or stop the crack from propagating further by blunting the crack front. As a consequence, pores might reduce or increase bone's fracture toughness (Christen et al., 2012; Donaldson et al., 2014; O'Brien et al., 2005; Taylor et al., 2007).

Computational techniques provide the means to assess the contribution of porosity on crack-growth independent of material and other structural differences. Crack initiation and propagation along a solution-dependent path can be analyzed using the eXtended Finite Element Method (XFEM) (Belytschko and Black, 1999; Moës et al., 1999; Sukumar et al., 2000). Crack location in XFEM is not confined to the boundaries of the mesh, and hence, there is no need of re-meshing (like in traditional FEM) or specifying a pre-defined path for crack growth. XFEM has been used to explore crack propagation on osteonal bone at the macro-scale (Feerick et al., 2013), micro-scale (Abdel-Wahab et al., 2012; Gao et al., 2013; Li et al., 2013b; Vergani et al., 2014) and from a multi-scale perspective (Budyn et al., 2008; Budyn and Hoc, 2007). Previous studies have used XFEM in the commercial software Abaqus to explore the effect of voids on the stress intensity factor (Jiang et al., 2014; Singh et al., 2011) or on neighboring cracks (Haboussa et al., 2011). However, these studies have not considered the propagation of cracks into and through the voids, which is not straightforward in Abaqus-XFEM.

Our objective was to establish a suitable modelling technique to propagate cracks through pores using Abaqus-XFEM. In order to test the different techniques, 2D models were created using images of the transversal topology of intra-cortical porosity of the *oim* mouse model of osteogenesis imperfecta, or brittle bone disease. *Oim*$^{-/-}$ bones have altered micro-porosity when compared to their wild-type controls (*oim*$^{+/+}$) (Carriero et al., 2014b), which might contribute to their brittle behavior (Carriero et al., 2014c). Hence, *oim* bones provide an excellent platform to explore the influence of real intra-cortical porosity on crack propagation.

2. Materials and methods

2.1. Extended Finite Element Method (XFEM)

We used XFEM capability in Abaqus (v 6.12, Dassault Systemes 2012) to model crack growth. In XFEM, cracks are modeled by adding ‘enrichment functions’ to the classical finite element nodal displacement functions (Figure 1a). The nodes where the enrichment term has been added are referred to as enrichment regions. Damage initiation and evolution are implemented in the enrichment regions according to the cohesive segment method (Moës and Belytschko, 2002; Remmers et al., 2003), as represented in Figure 1b. When the adopted failure criterion is met, damage is initiated and degradation of traction strength occurs until failure, when the crack opens. The area under the cohesive traction and crack opening curve G_c (Figure 1b) represents the critical value of fracture energy required to make the crack grow. Reviews about the theory behind XFEM can be found in (Fries and Belytschko, 2010; Karihaloo and Xiao, 2003; Yazid et al., 2009).

2.2. XFEM to model crack propagation through pores

There are difficulties associated with the propagation of cracks through pores when using XFEM in the commercial software Abaqus. According to the documentation of Abaqus 6.12:

'*Within an enrichment region* – which is the domain where the damage criteria is implemented - *a new crack initiation check is performed only after all existing cracks have completely separated. This may result in the abrupt appearance of multiple cracks.*' (Abaqus 6.12 documentation, 2012).

The effects of this are represented in Figure 2, where a square plate with an initial notch and one hole is subjected to tension in the horizontal direction. The whole plate corresponds to one enrichment region, where damage initiation is set to a maximum principal stress of 50 MPa. As tension is applied to the model and the crack propagates, new cracks should appear in the elements where the maximum principal stress reaches the critical value of 50 MPa (the areas shaded in grey in Figure 2). However, this is not the case. In Frame 209, the maximum principal stresses around the hole already exceed the 50 MPa but there are no new cracks starting at these grey regions. Instead, the existing crack keeps growing until it reaches the hole (Frame 448). The hole is considered as a boundary of the enrichment region; thus, after the existing crack reaches the hole, a new crack initiation check is performed. When this happens, there is a big area on the other side of the hole where the damage initiation criterion is met, which results in the abrupt appearance of multiple cracks from Frame 448 to Frame 449.

To overcome this limitation, here we consider two approaches (Figure 3). The first method consists of assigning void material properties to the holes (with Young's modulus, $E_{void} << E_{plate}$) so that the crack is free to propagate through the holes without reaching the boundary of the enrichment region, hence avoiding the abrupt appearance of multiple cracks

(Besdo and Vashishth, 2012; Li et al., 2013a). The second method is a novel approach where multiple partitions are employed and multiple enrichment regions are assigned with independent crack growth possibilities.

These two modelling techniques were tested using 2D models of the vascular porosity of healthy *oim*$^{+/+}$ and brittle *oim*$^{-/-}$ cortical bone.

2.3. Model setup

The topology of transverse cross-sections of healthy *oim*$^{+/+}$ and brittle *oim*$^{-/-}$ tibial mid-diaphysis was captured with synchrotron radiation-based computed tomography (CT) at the Swiss Light Source (Carriero et al., 2014b) and used to create 2D models of vascular and lacunar porosity (Figure 4). Regions (0.16 x 0.24 mm) containing vascular canals were chosen (red boxes in Figure 4). A frame (25 µm thick) of non-porous material was introduced around the model, in order to minimize the influence of the boundary conditions on the failure analysis. A notch (a_0 = 30 µm) was placed in the center of the lower edge and a displacement (δ = 2 µm) was applied perpendicular to the notch (Figure 4). The left edge was constraint in the direction of the applied displacement (x-direction). Four-node bilinear plane-strain quadrilateral elements with reduced integration (CPE4R) were used in the majority of the model and three-node linear plane-strain triangle elements (CPE3) were employed in the edges. The average element size ranged from 0.5 µm around the pores to 2 µm in the edges.

Traditional FEM was first run considering both vascular and lacunar porosities to identify regions of high stresses, which should roughly correspond to regions of crack initiation (Figure 5). The areas of maximum principal stress were located around the vascular pores. Hence, in order to keep the model simple, only vascular canals were considered in the XFEM simulations.

Two XFEM modelling approaches were tested (Figure 6). For the first method, void material properties were assigned to vascular canals and only one enrichment region was considered. In the second method, several partitions were made and multiple enrichment regions were assigned. In order to define the boundaries of the enrichment regions, a 'trial and error' approach was used. Initially, all the pores were divided by partitions to enable the initiation of cracks below and above the pore (where highest stresses were expected). The rest of the partitions were defined progressively looking at maximum principal stress maps until a crack would initiate in all the elements where the damage initiation criterion was met.

2.4. Material properties

In both the above mentioned models, the cohesive segment method was used with maximum principal stress failure criterion for damage initiation and an energy based damage evolution law for crack propagation (Abdel-Wahab et al., 2012; Feerick et al., 2013). Cortical bone damage properties used in the literature vary between 40-150 MPa for maximum principal stress (in tensile) and 0.2-3 N/mm for fracture energy (Abdel-Wahab et al., 2012; Feerick et al., 2013; Gao et al., 2013; Mischinski and Ural, 2011). In this study, bone was considered isotropic linear elastic and homogeneous and the same material properties were assigned for $oim^{-/-}$ and $oim^{+/+}$, to evaluate the effect of porosity only (Table 1). Hard contact was implemented on the faces of the elements split by the crack, to prevent non-physical over closure, with a coefficient of friction of 0.3 (Feerick et al., 2013).

3. Results

The crack propagation path for the four models is shown in Figure 7. When material properties were assigned to the vascular pores, only one crack propagated through the model (Figure 7, left). In contrast, when multiple enrichment regions were assigned, several cracks started progressively close to the vascular pores (Figure 7, right).

The reaction force on the left edge was computed against the applied displacement (Figure 8). The force-displacement curves showed that when void material properties were assigned to the pores, the reaction force was bigger in the *oim*$^{-/-}$ bones (Figure 8, left). However, when multiple partitions were employed, *oim*$^{-/-}$ bones showed smaller reaction forces than healthy *oim*$^{+/+}$ bones (Figure 8, right). Note that in both cases bone material properties were the same for the pathologic and wild-type models.

4. Discussion

The two modelling techniques yielded to different results, primarily the number of cracks which propagated. With only one enrichment zone (and filled pores), areas reached the damage criteria, but would not crack. This is due to the fact that in Abaqus-XFEM additional cracks cannot nucleate until all pre-existing cracks in an enriched feature have propagated (Abaqus 6.12 documentation, 2012). Thus, when filling the pores and considering the whole model as one enriched region, new cracks could not initiate until the existing crack from the notch had fully propagated reaching the boundary of the model (i.e. of the enriched region).

The sequential crack nucleation was captured when using the second technique. The multiple enrichment region approach indicated that the direction of the crack propagation was influenced by the vascular canals (Figure 7). This is in accordance with previous experimental studies in healthy mouse cortical bone which have demonstrated that the number of micro-cracks correlates significantly to the amount of vascular canals (Voide et al., 2011).

The measured reaction forces were also influenced by the modelling technique. The reaction force was higher in pathologic *oim*$^{-/-}$ than in control *oim*$^{+/+}$ bone when filling the pores, but lower when assigning multiple enrichment regions (Figure 8). The lower the reaction force, the easier it is for the crack to propagate. It is known that *oim*$^{-/-}$ bones exhibit decreased ultimate stress (Vanleene et al., 2012) and toughness (Carriero et al., 2014a, 2014c) than their wild-type controls (*oim*$^{+/+}$). Among other structural, mechanical and compositional alterations at different length-scales (Rodriguez-Florez et al., 2015), the altered micro-architecture of vascular canals found in *oim*$^{-/-}$ bone is expected to contribute to its brittleness (Carriero et al., 2014b, 2014c). Using an in-house software for crack propagation, we previously investigated the influence of the size and density of vascular canals on the crack extension in a schematic representation of the cortical porosity of *oim* bone: the crack propagates faster in presence of multiple smaller canals in *oim*$^{-/-}$ bone than in presence of a one single big canal in the wild-type counterpart *oim*$^{+/+}$. Smaller vascular canals increase the stresses on the remaining bone surface, offering less resistance to propagation (Carriero et al., 2014d). The lower reaction force measured with the multiple enrichment region technique is in accordance with those results. In contrast, the higher reaction forces measured with the first technique are the consequence of high stresses developed due to the lack of sequential crack nucleation, as shown in Figure 9.

Based on these results, the multiple enrichment region technique is recommended for future analysis of bone micro-porosity when using XFEM in Abaqus. However, there are some limitations that must be taken into account. First, it is cumbersome to create adequate partitions in the model, which will become increasingly difficult when including more and smaller pores, such as lacunar porosity, or modelling bone micro-porosity in 3D under mixed loads. Other general limitations are associated with the XFEM capabilities in Abaqus, as cracks cannot branch nor interact with each other (Abaqus 6.12 documentation, 2012). Despite these limitations, the current study introduced a new technique to investigate the crack/pore interaction in bone using commercial software.

5. Conclusion

This study explored the use of extended finite element models in Abaqus to investigate the influence of bone micro-porosity on crack formation and growth at the micro-scale. A new modelling technique based on multiple enrichment regions was suggested and it was compared to assigning void material properties to pores. When a complex topology of vascular porosity such as that in *oim* bone was modelled, filling the pores resulted in non-physiological propagation of the crack. In conclusion, the multiple enrichment region technique is necessary to capture progressive crack initiation and propagation in Abaqus-XFEM.

6. Acknowledgements

This study was supported by the Basque Government pre-doctoral fellowship (Spain). We thank Dr Adriana Paluszny for insightful discussions about fracture mechanics.

7. References

Abaqus 6.12 documentation, 2012. Simulia, Dassault Systemes. Providence, Rhode Island, US.

Abdel-Wahab, A.A., Maligno, A.R., Silberschmidt, V.V., 2012. Micro-scale modelling of bovine cortical bone fracture: Analysis of crack propagation and microstructure using X-FEM. Comput. Mater. Sci. 52, 128–135. doi:10.1016/j.commatsci.2011.01.021

Belytschko, T., Black, T., 1999. Elastic crack growth in finite elements with minimal remeshing. Int. J. Numer. Methods Eng. 45, 601–620. doi:10.1002/(SICI)1097-0207(19990620)45:5<601::AID-NME598>3.0.CO;2-S

Besdo, S., Vashishth, D., 2012. Extended Finite Element models of intracortical porosity and heterogeneity in cortical bone. Comput. Mater. Sci., Proceedings of the 21st International Workshop on Computational Mechanics of Materials (IWCMM 21) 64, 301–305. doi:10.1016/j.commatsci.2012.04.018

Budyn, É., Hoc, T., 2007. Multiple scale modeling for cortical bone fracture in tension using X-FEM. Eur. J. Comput. Mech. Eur. Mécanique Numér. 16, 213–236. doi:10.3166/remn.16.213-236

Budyn, E., Hoc, T., Jonvaux, J., 2008. Fracture strength assessment and aging signs detection in human cortical bone using an X-FEM multiple scale approach. Comput. Mech. 42, 579–591. doi:10.1007/s00466-008-0283-1

Buehler, M.J., 2007. Molecular nanomechanics of nascent bone: fibrillar toughening by mineralization. Nanotechnology 18, 295102. doi:10.1088/0957-4484/18/29/295102

Carriero, A., Bruse, J.L., Oldknow, K.J., Millán, J.L., Farquharson, C., Shefelbine, S.J., 2014a. Reference point indentation is not indicative of whole mouse bone measures of stress intensity fracture toughness. Bone 69, 174–179. doi:10.1016/j.bone.2014.09.020

Carriero, A., Doube, M., Vogt, M., Busse, B., Zustin, J., Levchuk, A., Schneider, P., Müller, R., Shefelbine, S.J., 2014b. Altered lacunar and vascular porosity in osteogenesis imperfecta mouse bone as revealed by synchrotron tomography contributes to bone fragility. Bone. doi:10.1016/j.bone.2013.12.020

Carriero, A., Zimmermann, E.A., Paluszny, A., Tang, S.Y., Bale, H., Busse, B., Alliston, T., Kazakia, G., Ritchie, R.O., Shefelbine, S.J., 2014c. How tough is Brittle Bone? Investigating Osteogenesis Imperfecta in Mouse Bone. J. Bone Miner. Res. Off. J. Am. Soc. Bone Miner. Res. doi:10.1002/jbmr.2172

Carriero A., Zimmermann, E.A.,Shefelbine, S.J., Ritchie, R.O, 2014d. A methodology for the investigation of toughness and crack propagation in mouse bone. J. Mech. Behav. Biomed. Mater. 39, 38-47. doi: 10.1016/j.jmbbm.2014.06.017

Christen, D., Levchuk, A., Schori, S., Schneider, P., Boyd, S.K., Müller, R., 2012. Deformable image registration and 3D strain mapping for the quantitative assessment of cortical bone microdamage. J. Mech. Behav. Biomed. Mater. 8, 184–193. doi:10.1016/j.jmbbm.2011.12.009

Donaldson, F., Ruffoni, D., Schneider, P., Levchuk, A., Zwahlen, A., Pankaj, P., Müller, R., 2014. Modeling microdamage behavior of cortical bone. Biomech. Model. Mechanobiol. 13, 1227–1242. doi:10.1007/s10237-014-0568-6

Feerick, E.M., Liu, X.C., McGarry, P., 2013. Anisotropic mode-dependent damage of cortical bone using the extended finite element method (XFEM). J. Mech. Behav. Biomed. Mater. 20, 77–89. doi:10.1016/j.jmbbm.2012.12.004

Fries, T.-P., Belytschko, T., 2010. The extended/generalized finite element method: An overview of the method and its applications. Int. J. Numer. Methods Eng. 84, 253–304. doi:10.1002/nme.2914

Gao, X., Li, S., Adel-Wahab, A., Silberschmidt, V., 2013. Effect of random microstructure on crack propagation in cortical bone tissue under dynamic loading. J. Phys. Conf. Ser. 451, 012033. doi:10.1088/1742-6596/451/1/012033

Gupta, H.S., Krauss, S., Kerschnitzki, M., Karunaratne, A., Dunlop, J.W.C., Barber, A.H., Boesecke, P., Funari, S.S., Fratzl, P., 2013. Intrafibrillar plasticity through mineral/collagen sliding is the dominant mechanism for the extreme toughness of antler bone. J. Mech. Behav. Biomed. Mater. 28, 366–382. doi:10.1016/j.jmbbm.2013.03.020

Haboussa, D., Grégoire, D., Elguedj, T., Maigre, H., Combescure, A., 2011. X-FEM analysis of the effects of holes or other cracks on dynamic crack propagations. Int. J. Numer. Methods Eng. 86, 618–636. doi:10.1002/nme.3128

Jiang, S., Du, C., Gu, C., Chen, X., 2014. XFEM analysis of the effects of voids, inclusions and other cracks on the dynamic stress intensity factor of a major crack. Fatigue Fract. Eng. Mater. Struct. 37, 866–882. doi:10.1111/ffe.12150

Karihaloo, B.L., Xiao, Q.Z., 2003. Modelling of stationary and growing cracks in FE framework without remeshing: a state-of-the-art review. Comput. Struct. 81, 119–129. doi:10.1016/S0045-7949(02)00431-5

Launey, M.E., Buehler, M.J., Ritchie, R.O., 2010. On the Mechanistic Origins of Toughness in Bone. Annu. Rev. Mater. Res. 40, 25–53. doi:10.1146/annurev-matsci-070909-104427

Li, S., Abdel-Wahab, A., Demirci, E., Silberschmidt, V.V., 2013a. Fracture process in cortical bone: X-FEM analysis of microstructured models. Int. J. Fract. 184, 43–55. doi:10.1007/s10704-013-9814-7

Li, S., Abdel-Wahab, A., Silberschmidt, V.V., 2013b. Analysis of fracture processes in cortical bone tissue. Eng. Fract. Mech. 110, 448–458. doi:10.1016/j.engfracmech.2012.11.020

Mischinski, S., Ural, A., 2011. Finite Element Modeling of Microcrack Growth in Cortical Bone. J. Appl. Mech. 78, 041016–041016. doi:10.1115/1.4003754

Moës, N., Belytschko, T., 2002. Extended finite element method for cohesive crack growth. Eng. Fract. Mech. 69, 813–833. doi:10.1016/S0013-7944(01)00128-X

Moës, N., Dolbow, J., Belytschko, T., 1999. A finite element method for crack growth without remeshing. Int. J. Numer. Methods Eng. 46, 131–150. doi:10.1002/(SICI)1097-0207(19990910)46:1<131::AID-NME726>3.0.CO;2-J

Nalla, R.K., Kruzic, J.J., Kinney, J.H., Ritchie, R.O., 2005. Mechanistic aspects of fracture and R-curve behavior in human cortical bone. Biomaterials 26, 217–231. doi:10.1016/j.biomaterials.2004.02.017

O'Brien, F.J., Taylor, D., Clive Lee, T., 2005. The effect of bone microstructure on the initiation and growth of microcracks. J. Orthop. Res. 23, 475–480. doi:10.1016/j.orthres.2004.08.005

Remmers, J.J.C., Borst, R. de, Needleman, A., 2003. A cohesive segments method for the simulation of crack growth. Comput. Mech. 31, 69–77. doi:10.1007/s00466-002-0394-z

Ritchie, R.O., Buehler, M.J., Hansma, P., 2009. Plasticity and toughness in bone. Phys. Today 62, 41–47. doi:10.1063/1.3156332

Rodriguez-Florez, N., Garcia-Tunon, E., Mukadam, Q., Saiz, E., Oldknow, K.J., Farquharson, C., Millán, J.L., Boyde, A., Shefelbine, S.J., 2015. An Investigation of the Mineral in Ductile and Brittle Cortical Mouse Bone. J. Bone Miner. Res. 30, 786–795. doi:10.1002/jbmr.2414

Singh, I.V., Mishra, B.K., Bhattacharya, S., 2011. XFEM simulation of cracks, holes and inclusions in functionally graded materials. Int. J. Mech. Mater. Des. 7, 199–218. doi:10.1007/s10999-011-9159-1

Sukumar, N., Moës, N., Moran, B., Belytschko, T., 2000. Extended finite element method for three-dimensional crack modelling. Int. J. Numer. Methods Eng. 48, 1549–1570. doi:10.1002/1097-0207(20000820)48:11<1549::AID-NME955>3.0.CO;2-A

Taylor, D., Hazenberg, J.G., Lee, T.C., 2007. Living with cracks: Damage and repair in human bone. Nat. Mater. 6, 263–268. doi:10.1038/nmat1866

Turnbull, T.L., Baumann, A.P., Roeder, R.K., 2014. Fatigue microcracks that initiate fracture are located near elevated intracortical porosity but not elevated mineralization. J. Biomech. 47, 3135–3142. doi:10.1016/j.jbiomech.2014.06.022

Ural, A., Vashishth, D., 2014. Hierarchical perspective of bone toughness – from molecules to fracture. Int. Mater. Rev. 59, 245–263. doi:10.1179/1743280414Y.0000000031

Vanleene, M., Porter, A., Guillot, P.-V., Boyde, A., Oyen, M., Shefelbine, S., 2012. Ultra-structural defects cause low bone matrix stiffness despite high mineralization in osteogenesis imperfecta mice. Bone. doi:10.1016/j.bone.2012.03.007

Vardakastani, V., Saletti, D., Skalli, W., Marry, P., Allain, J.M., Adam, C., 2014. Increased intra-cortical porosity reduces bone stiffness and strength in pediatric patients with osteogenesis imperfecta. Bone 69, 61–67. doi:10.1016/j.bone.2014.09.003

Vergani, L., Colombo, C., Libonati, F., 2014. Crack Propagation in Cortical Bone: A Numerical Study. Procedia Mater. Sci., 20th European Conference on Fracture 3, 1524–1529. doi:10.1016/j.mspro.2014.06.246

Voide, R., Schneider, P., Stauber, M., van Lenthe, G.H., Stampanoni, M., Müller, R., 2011. The importance of murine cortical bone microstructure for microcrack initiation and propagation. Bone 49, 1186–1193. doi:10.1016/j.bone.2011.08.011

Wang, R., Gupta, H.S., 2011. Deformation and Fracture Mechanisms of Bone and Nacre. Annu. Rev. Mater. Res. 41, 41–73. doi:10.1146/annurev-matsci-062910-095806

Yazid, A., Abdelkader, N., Abdelmadjid, H., 2009. A state-of-the-art review of the X-FEM for computational fracture mechanics. Appl. Math. Model. 33, 4269–4282. doi:10.1016/j.apm.2009.02.010

Yeni, Y.N., Brown, C.U., Wang, Z., Norman, T.L., 1997. The influence of bone morphology on fracture toughness of the human femur and tibia. Bone 21, 453–459. doi:10.1016/S8756-3282(97)00173-7

Zimmermann, E.A., Gludovatz, B., Schaible, E., Busse, B., Ritchie, R.O., 2014. Fracture resistance of human cortical bone across multiple length-scales at physiological strain rates. Biomaterials 35, 5472–5481. doi:10.1016/j.biomaterials.2014.03.066

Zimmermann, E.A., Schaible, E., Bale, H., Barth, H.D., Tang, S.Y., Reichert, P., Busse, B., Alliston, T., Ager, J.W., Ritchie, R.O., 2011. Age-related changes in the plasticity and toughness of human cortical bone at multiple length scales. Proc. Natl. Acad. Sci. doi:10.1073/pnas.1107966108

Figure captions

Figure 1: a) Classical FEM nodes 'enriched' in the nodes belonging to elements cut by the crack (circles in red). b) Traction-separation law assigned to the enriched nodes. The area under the curve is the fracture energy required to propagate the crack, G_c.

Figure 2: A plate with an initial vertical notch subjected to horizontal tension. The damage initiation criterion is set to a maximum principal stress of 50 MPa. As the crack propagates (Frame 209), there are grey-shaded areas (pointed by the arrow) in which the damage initiation criterion is met. However, a damage initiation check is not performed until the existing crack reaches the hole. There is an abrupt appearance of multiple cracks from Frame 448 to 449.

Figure 3: Two techniques to model crack growth through a hole: Method 1) Assigning material properties with reduced Young's modulus, *E*, to the void; Method 2) Employing partitions and assigning different enrichment regions, so that the damage initiation check is performed in each of the regions independently.

Figure 4: Model geometry setup. The topologies of transverse cross-sections of healthy $oim^{+/+}$ and brittle $oim^{-/-}$ tibial mid-diaphysis were captured with synchrotron radiation-based CT (Carriero et al., 2014b) and used to create 2D models of intra-cortical porosity. A notch a_0 was placed and a displacement δ was applied on the right edge, while the left edge was constraint in the x-direction.

Figure 5: Classical FE models of $oim^{+/+}$ and $oim^{-/-}$ after applying a displacement of 2 μm to the right edge. Brittle bone reached higher stresses than healthy bone. Regions of maximum stresses correspond to areas around the vascular pores.

Figure 6: $Oim^{+/+}$ and $oim^{-/-}$ models of vascular canals with partitions. In method one, there is only one enrichment region assigned to the model and the pores are filled. In the second method, multiple partitions are defined and different enrichment regions are assigned to each partition, while the pores are kept empty.

Figure 7: Crack propagation (in red) in $oim^{+/+}$ and $oim^{-/-}$ models of vascular pores. Only one crack propagates when material properties are assigned to voids, while multiple cracks propagate following the vascular pores when using the multiple enrichment region technique.

Figure 8: Reaction force on the left edge against the applied displacement on the right edge of the model. With the first technique (left), *oim*$^{-/-}$ model exhibits a bigger reaction force, while with the second technique (right) *oim*$^{-/-}$ has lower reaction forces than healthy *oim*$^{+/+}$.

Figure 9: Crack growth during the applied displacement δ in the *oim*$^{-/-}$ model where void material properties were assigned to pores. Although the critical maximum principal stress of 50 MPa is reached (light blue and above) around the pores, new cracks do not initiate. Note that pores are shown white to aid in the visualization but they are indeed filled.

Tables

Table 1: Material properties assigned to $oim^{+/+}$ and $oim^{-/-}$ models.

		Bone	Pore
Elastic properties	Young's modulus, E (MPa)	10000	10
	Poisson's ratio, v	0.15	0.15
Damage properties	Max. principal stress, σ_{max} (MPa)	50	50
	Fracture energy, G_c (N/mm)	0.238	0.238

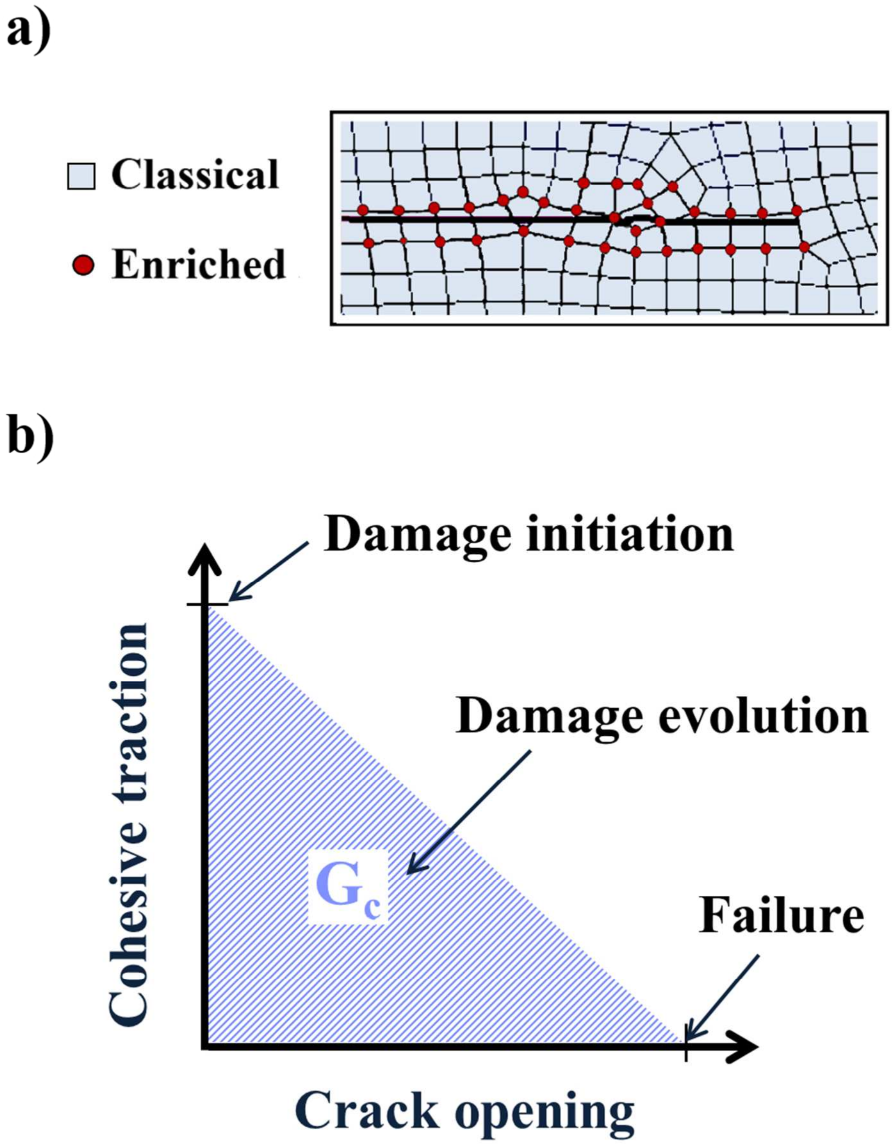

Figure 1: a) Classical FEM nodes 'enriched' in the nodes belonging to elements cut by the crack (circles in red). b) Traction-separation law assigned to the enriched nodes. The area under the curve is the fracture energy required to propagate the crack, Gc.
90x106mm (300 x 300 DPI)

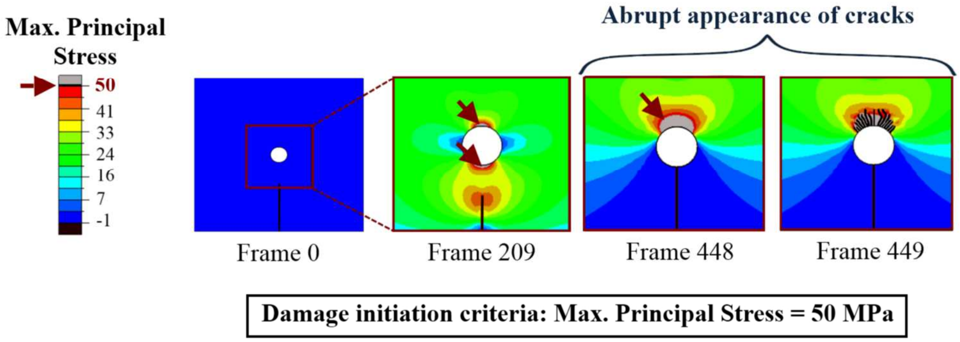

Figure 2: A plate with an initial vertical notch subjected to horizontal tension. The damage initiation criterion is set to a maximum principal stress of 50 MPa. As the crack propagates (Frame 209), there are grey-shaded areas (pointed by the arrow) in which the damage initiation criterion is met. However, a damage initiation check is not performed until the existing crack reaches the hole. There is an abrupt appearance of multiple cracks from Frame 448 to 449.
180x66mm (300 x 300 DPI)

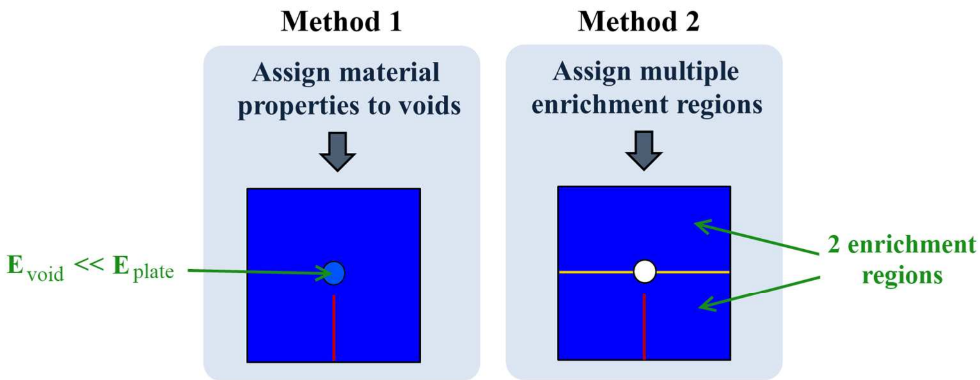

Figure 3: Two techniques to model crack growth through a hole: Method 1) Assigning material properties with reduced Young's modulus, E, to the void; Method 2) Employing partitions and assigning different enrichment regions, so that the damage initiation check is performed in each of the regions independently.
149x60mm (300 x 300 DPI)

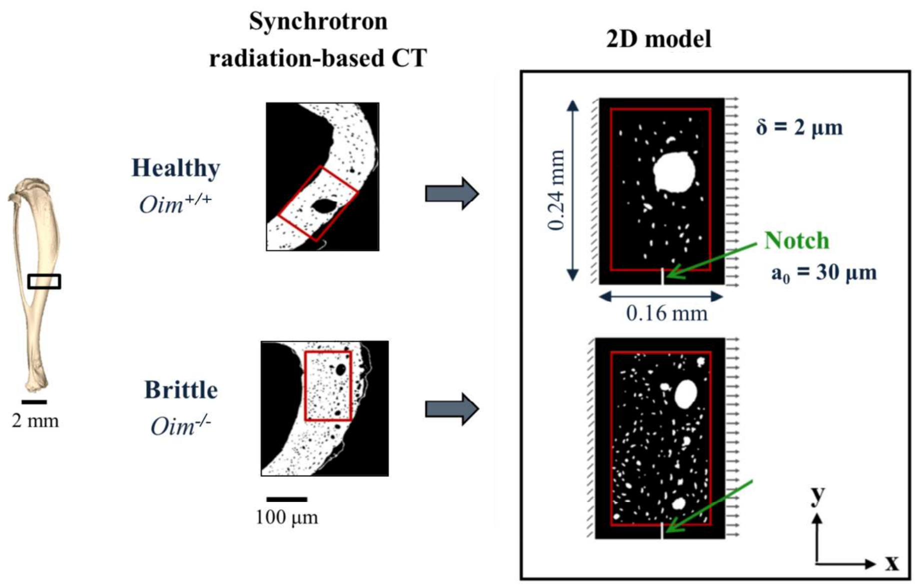

Figure 4: Model geometry setup. The topologies of transverse cross-sections of healthy oim+/+ and brittle oim-/- tibial mid-diaphysis were captured with synchrotron radiation-based CT (Carriero et al., 2014b) and used to create 2D models of intra-cortical porosity. A notch a0 was placed and a displacement δ was applied on the right edge, while the left edge was constraint in the x-direction.
159x96mm (300 x 300 DPI)

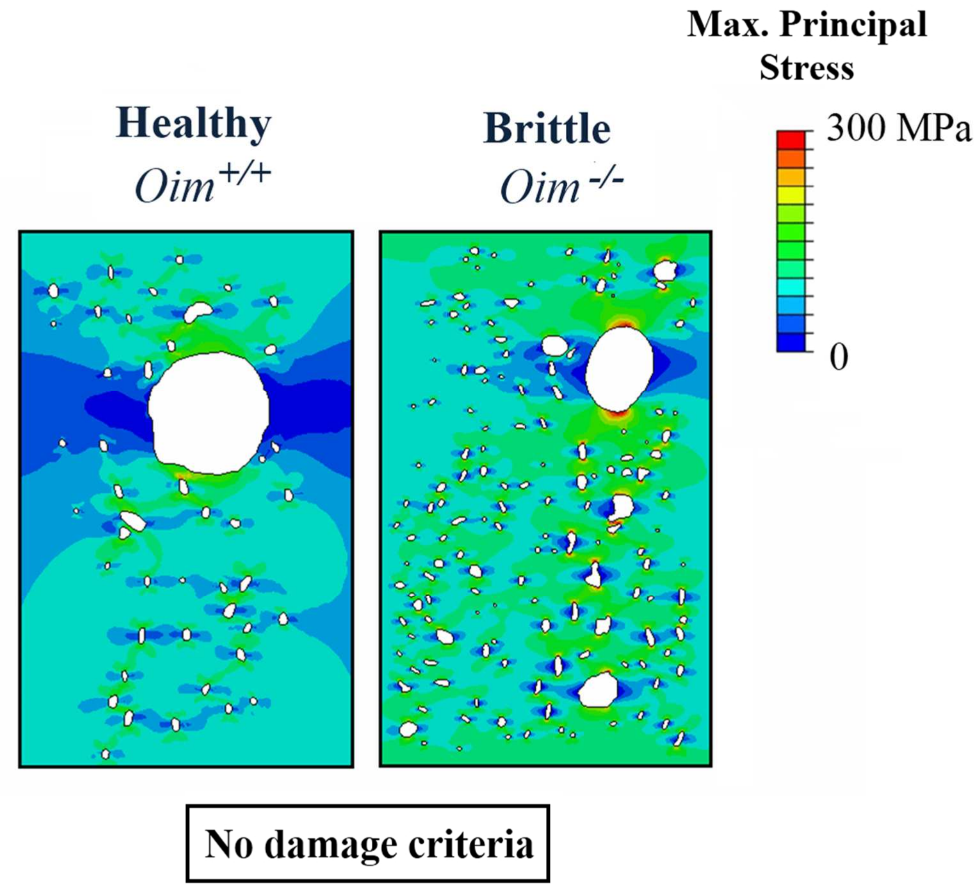

Figure 5: Classical FE models of oim+/+ and oim-/- after applying a displacement of 2 μm to the right edge. Brittle bone reached higher stresses than healthy bone. Regions of maximum stresses correspond to areas around the vascular pores.
90x82mm (300 x 300 DPI)

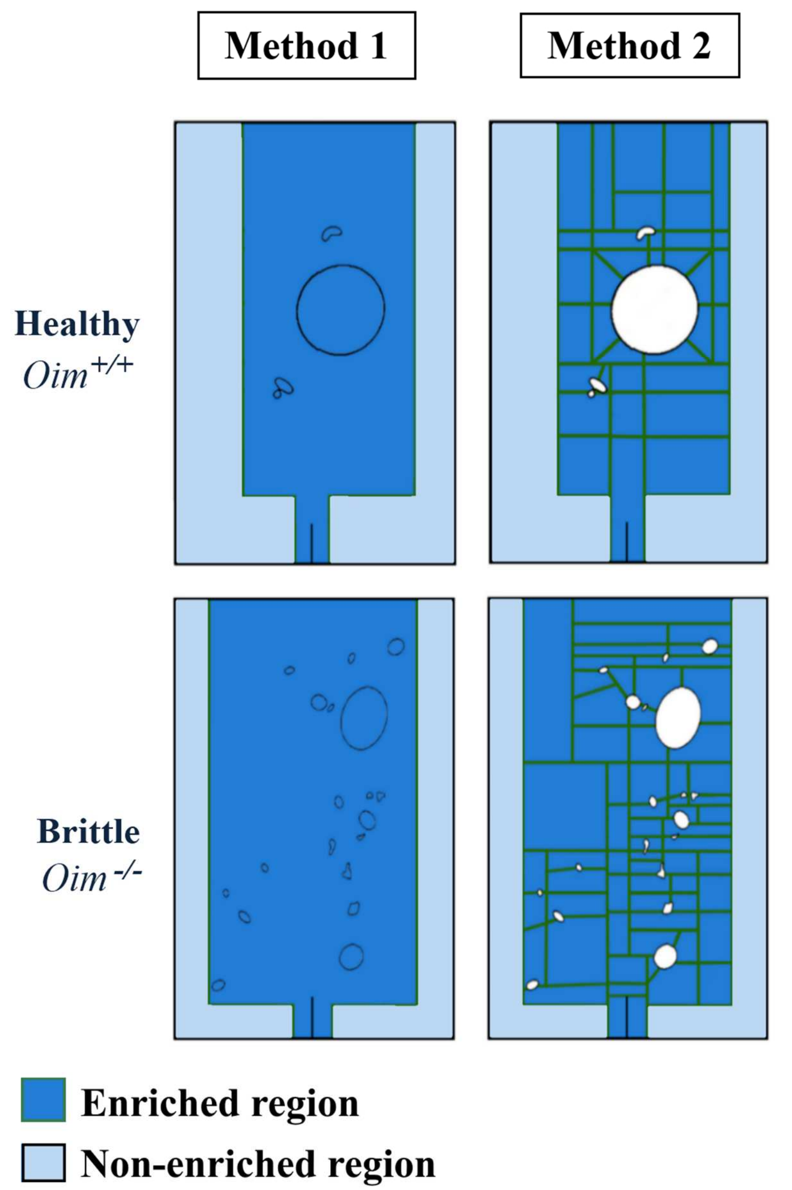

Figure 6: Oim+/+ and oim-/- models of vascular canals with partitions. In method one, there is only one enrichment region assigned to the model and the pores are filled. In the second method, multiple partitions are defined and different enrichment regions are assigned to each partition, while the pores are kept empty.
90x133mm (300 x 300 DPI)

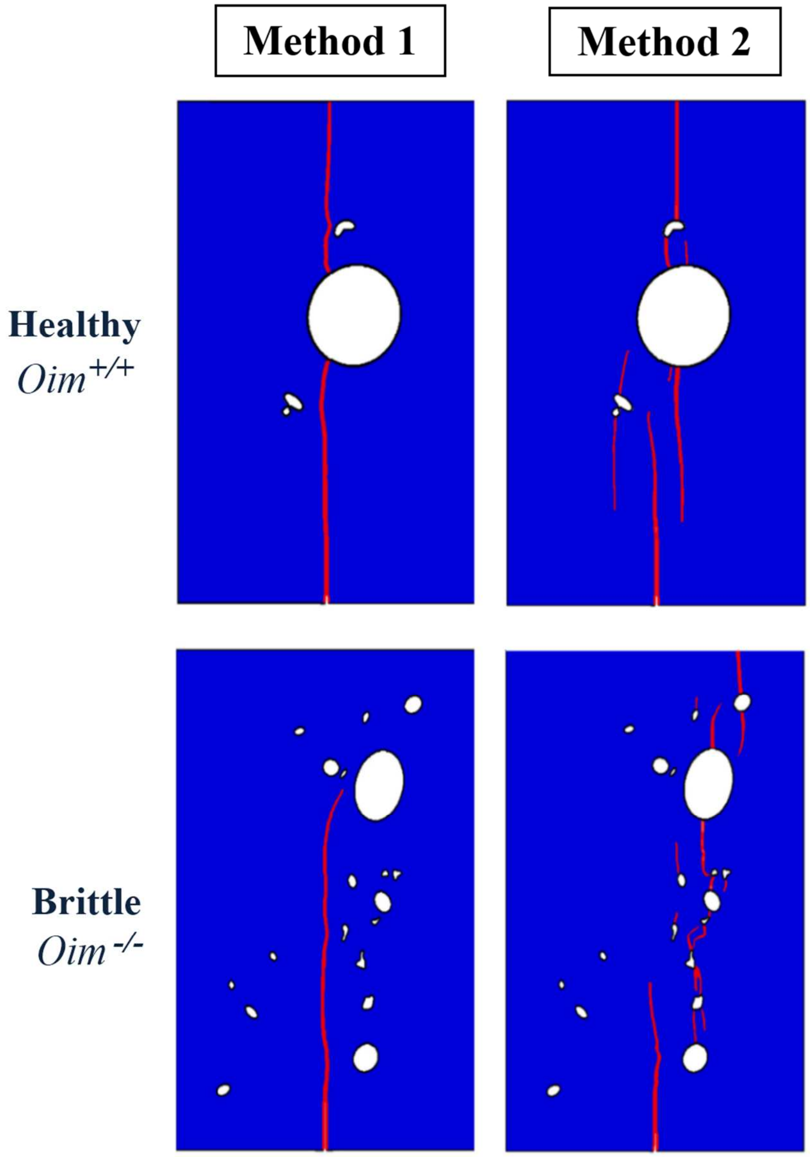

Figure 7: Crack propagation (in red) in oim+/+ and oim-/- models of vascular pores. Only one crack propagates when material properties are assigned to voids, while multiple cracks propagate following the vascular pores when using the multiple enrichment region technique.
90x126mm (300 x 300 DPI)

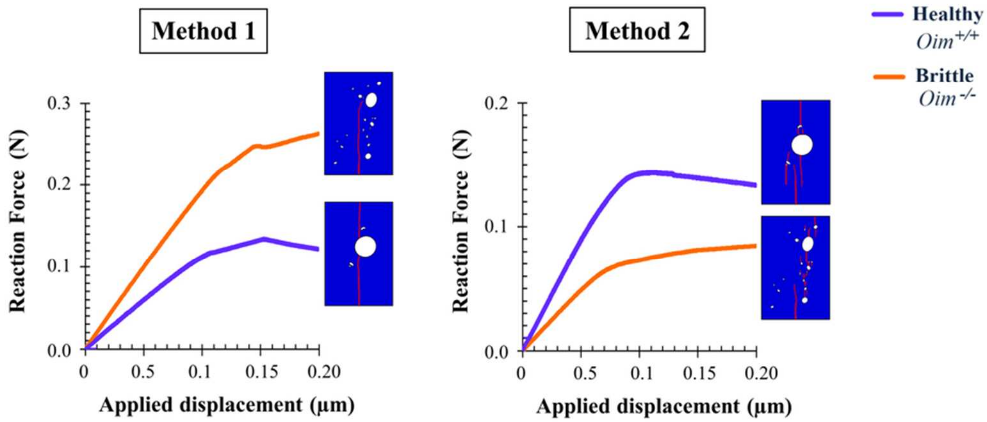

Figure 8: Reaction force on the left edge against the applied displacement on the right edge of the model. With the first technique (left), oim-/- model exhibits a bigger reaction force, while with the second technique (right) oim-/- has lower reaction forces than healthy oim+/+.
79x34mm (300 x 300 DPI)

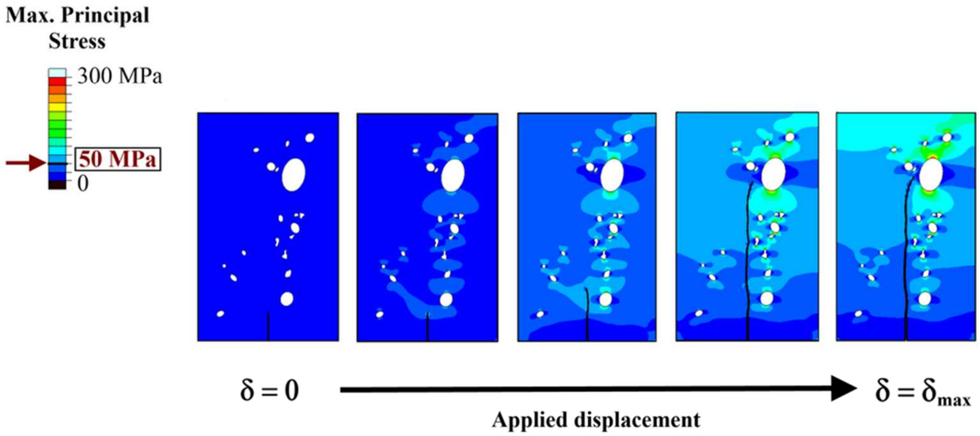

Figure 9: Crack growth during the applied displacement δ in the oim-/- model where void material properties were assigned to pores. Although the critical maximum principal stress of 50 MPa is reached (light blue and above) around the pores, new cracks do not initiate. Note that pores are shown white to aid in the visualization but they are indeed filled.
82x37mm (300 x 300 DPI)